JACS ARTICLES

Published on Web 01/05/2010

Polarity-Sensitive Coumarins Tailored to Live Cell Imaging

Giovanni Signore,*[,†] Riccardo Nifosì,[‡] Lorenzo Albertazzi,[†,‡] Barbara Storti,[†,‡] and Ranieri Bizzarri*[,†,‡]

NEST, CNR-INFM, p.za San Silvestro 12, 56127 Pisa, Italy, NEST, Scuola Normale Superiore, and IIT@NEST, Center for Nanotechnology Innovation, p.za San Silvestro 12, I-56127 Pisa, Italy

Received June 19, 2009; E-mail: giovanni.signore@iit.it; r.bizzarri@sns.it

Abstract: Polarity-dependent fluorescent probes are recently attracting interest for high-resolution cell imaging. Following a stepwise rational approach, we prepared and tested a toolbox of new coumarin derivatives tailored to *in vivo* imaging applications. Our compounds are characterized by a donor−(coumarin core)−acceptor molecular structure, where the electron donor is represented by alkylether or naphthyl groups, and the electron acceptor is represented by benzothiazene and cyano groups. Prior to synthesis, the substitution patterns were screened by computational methods to provide functional fluorescent derivatives easy to synthesize, and with excitation in the visible region of spectrum. We set up a robust synthetic procedure tunable on the substitution patterns to achieve. These coumarins possess excellent fluorescence quantum yields (up to 0.95), high molar extinction coefficients (up to 46,000 M^{-1} cm^{-1}), and large Stokes shifts. Furthermore, they display strong solvatochromism, being almost non-emissive in water and very fluorescent in less polar media (up to 780-fold enhancement in brightness). The solvatochromism of these compounds can be accounted for by a photophysical method encompassing two communicating excited states. When tested on cultured cells, the results showed that the developed coumarins were not harmful and their photophysical properties were unchanged compared to free solution. According to the determined solvatochromic properties, the coumarin fluorescence was detected only in the most lipophilic environments of the cell. The prepared compounds represent remarkable tools to investigate subtle biochemical processes in the cell environment after appropriate conjugation to biomolecules, and at the same time constitute the basis for further engineering of a new generation of biosensors.

1. Introduction

Cell behavior is regulated by transient activation of protein activities in specific subcellular regions. The recent development of highly fluorescent probes tailored to the cellular environment and of high-resolution imaging techniques allows monitoring protein activity in living cells by direct optical methods.[1] Members of the green fluorescent protein family (GFPs) are particularly impressive nanoprobes for *in vivo* studies, owing to their genetically encoded fluorescence.[2,3] Effective chemical methods were developed to link functional organic dyes, often more fluorescent and resistant to photodegradation than GFPs, to proteins *in vivo*.[4] In most cases, however, genetic modification of the target protein is needed for the probe binding; the least invasive methods involve adding non-native peptide sequences of 6−20 amino acids to the target protein. Thus, the detection of protein activity in the true native state or after post-translational modification is intrinsically impossible. The use of multicomponent molecular species penetrating into the cell and capable of recognizing selectively a certain state of the target protein (universal biosensors) could overcome this problem. Peptide sequences able to convey into the cell a tailored molecular cargo and/or to bind to a specific protein configuration are now widely investigated for this purpose.[5] How to signal the protein recognition event, however, is still unclear. An elegant answer to this question considers organic dyes whose optical properties are *sensitive* to the surrounding environment (solvatochromic probes).[6−19] According to this approach, the

† IIT@NEST, Center for Nanotechnology Innovation, I-56127 Pisa, Italy.
‡ NEST, Scuola Normale Superiore and CNR-INFM, I-56127 Pisa, Italy.

(1) Petty, H. R. *Microsc. Res. Tech.* **2007**, *70*, 687–709.
(2) Miyawaki, A. *Neuron* **2005**, *48*, 189–199.
(3) Bizzarri, R.; Arcangeli, C.; Arosio, D.; Ricci, F.; Faraci, P.; Cardarelli, F.; Beltram, F. *Biophys. J.* **2006**, *90*, 3300–3314.
(4) Prescher, J. A.; Bertozzi, C. R. *Nat. Chem. Biol.* **2005**, *1*, 13–21.
(5) Cardarelli, F.; Serresi, M.; Bizzarri, R.; Beltram, F. *Traffic* **2008**, *9*, 528–539.
(6) Toutchkine, A.; Kraynov, V.; Hahn, K. M. *J. Am. Chem. Soc.* **2003**, *125*, 4132–4145.
(7) Nalbant, P.; Hodgson, L.; Kraynov, V.; Toutchkine, A.; Hahn, K. M. *Science* **2004**, *305*, 1615–1619.
(8) Cohen, B. E.; Pralle, A.; Yao, X.; Swaminath, G.; Gandhi, C. S.; Jan, Y. N.; Kobilka, B. K.; Isacoff, E. Y.; Jan, L. Y. *Proc. Natl. Acad. Sci. U.S.A.* **2005**, *102*, 965–970.
(9) Kobiilka, B. K.; Gether, U. *Methods Enzymol.* **2002**, *343*, 170–182.
(10) Mannuzzu, L. M.; Moronne, M. M.; Isacoff, E. Y. *Science (Washington, DC, U.S.)* **1996**, *271*, 213–216.
(11) Hanouni, P.; Gryczynski, Z.; Steenhuis, J.; Lee, T. W.; Farrens, D. L.; Lakowicz, J. R.; Kobilka, B. K. *J. Biol. Chem.* **2001**, *276*, 24433–24436.
(12) Cohen, B. E.; McAnaney, T. B.; Park, E. S.; Jan, Y. N.; Boxer, S. G.; Jan, L. Y. *Science* **2002**, *296*, 1700–1703.
(13) Lavis, L. D.; Raines, R. T. *ACS Chem. Biol.* **2008**, *3*, 142–155.
(14) Venkatraman, P.; Nguyen, T. T.; Sainlos, M.; Bilsel, O.; Chitta, S.; Imperiali, B.; Stern, L. *Nat. Chem. Biol.* **2007**, *3*, 222–228.
(15) Fülöp, A.; Arian, D.; Lysenko, A.; Mokhir, A. *Bioorg. Med. Chem. Lett.* **2009**, *19*, 3104–3107.
(16) Sainlos, M.; Iskenderian, W. S.; Imperiali, B. *J. Am. Chem. Soc.* **2009**, *131*, 6680–6682.
(17) Dai, Z.; Dulyaninova, N. G.; Kumar, S.; Bresnick, A. R.; Lawrence, D. S. *Chem. Biol.* **2007**, 1254–1260.

 10.1021/ja9050444

recognition signal comes from a solvatochromic prosthetic group able to sense the polarity change associated with binding. Reasonably, it should be located at a site close enough to the binding region of the biosensor (where changes in polarity necessarily occur) but not too close, so that it does not hamper the recognition and binding process.

In past years, solvatochromic dyes have been extensively employed in selective staining of many subcellular domains. Notably, solvatochromic FM dyes are widely employed as membrane-staining agents, since they localize preferentially on cell membrane, where their fluorescence is enhanced.[20] However, the development of solvatochromic dyes as polarity probes to investigate protein binding, membrane rearrangement, and other biological processes has not evolved to its full potential.

Fluorescent coumarins are attractive fluorophores, as they are characterized by high quantum yields (up to 0.90),[21] high extinction coefficients (10,000−40,000),[22,23] large Stokes shifts (up to 160 nm),[24] and can be engineered to respond to their environment polarity (solvatochromic probes).[25−27] These properties promoted their use as dyes,[28,21,29] sensors for metal cations,[30−34] and dopants for OLEDs.[35,36] The well-known commercial fluorophores Alexa 350 and Alexa 430 are based on a coumarin core.[37] Recently, coumarins were thoroughly investigated in view of synthesizing new probes for biological applications, in particular for the imaging of living cells.[38−48] In spite of their relevance as biosensors, however, no studies describing solvatochromic coumarins tailored to probe the different polarity properties of biological environments in cultured cells have been yet reported.

A powerful method to confer solvatochromic properties to aromatic fluorophores involves the concomitant functionalization with electron-donor (D) and electron-acceptor (A) groups. This effect is related to the large dipole moment present in such structures and its significant variations between the ground and the excited state. In such a case, the excited state is often referred to as intramolecular charge transfer (ICT). The change in solvation energy between polar and apolar environments accounts for the shift in intensity and/or wavelength in their absorption and fluorescence spectra.[49] Alternatively, the ICT state can evolve along the energy landscape to excited states of different nature following a process that is strongly influenced by the surrounding polarity.

The aromatic core of coumarin is particularly suitable for the introduction of D and A groups, as the most common synthetic pathway involves the use of hydroxy aldehydes and 2-aryl substituted acetates. Both of these aromatic subunits can be easily functionalized with A or D groups. This work will present the synthesis and spectroscopic analysis of new solvatochromic coumarins for intracellular use bearing one A group in position 3, and D groups in positions 5, 6, 7 and/or 8.

Concerning position 3, our choice fell on a benzothiazene group, owing to its electron-withdrawing aromatic system capable also to extend electron conjugation. Amino substituents are excellent D groups, and would represent a good choice for the electron-rich part of the fluorophore. These substituents, however, bring about significant drawbacks. Indeed, aromatic amino groups are quite reactive and may undergo chemical processes that hamper their further functionalization and/or strongly affect the solvatochromic outcome (e.g., protonation of the amino group strongly decreases its electron-donating capability). Our selection for the positions 5−8 fell on oxygen-based D groups, which essentially overcome these limitations while retaining most of the electron-donating properties of amino substituents. Additionally, we explored the possibility to incorporate a further aromatic ring to increase electronic conjugation. In the following, we shall show that these new fluorophores display high sensitivity to the environmental polarity combined with good-to-excellent brightness and are indeed suitable for intracellular use.

2. Results

2.1. Computational Screening of Coumarin Compounds. Preliminarily to any experimental step, a computational analysis by density functional theory (DFT/B3LYP) was performed to identify interesting substitution donor−(coumarin core)−acceptor

(18) Loving, G.; Imperiali, B. *J. Am. Chem. Soc.* **2008**, *130*, 13630–13638.
(19) Volodymyr, S. V.; Klymchenko, A. S.; de Rocquigny, H.; Mély, Y. *Nucleic Acids Res.* **2009**, *37*, e25.
(20) Bolte, S.; Talbot, C.; Boutte, Y.; Catrice, O.; Read, N. D.; Satiat-Jeunemaitre, B. *J. Microsc.* **2004**, *214*, 159–173.
(21) Turki, H.; Abid, S.; Fery-Forgues, S.; El Gharbi, R. *Dyes Pigm.* **2007**, *73*, 311–316.
(22) Christie, R. M.; Lui, C.-H. *Dyes Pigm.* **2000**, *47*, 79–89.
(23) Wolfbeis, O. S.; Koller, E.; Hochmuth, P. *Bull. Chem. Soc. Jpn.* **1985**, *58*, 731–734.
(24) Elangovan, A.; Lin, J.-H.; Yang, S.-W.; Hsu, H.-Y.; Ho, T.-I. *J. Org. Chem.* **2004**, *69*, 8086–8092.
(25) Hirano, T.; Hiromoto, K.; Kagechika, H. *Org. Lett.* **2007**, *9*, 1315–1318.
(26) Turki, H.; Abid, S.; El Gharbi, R.; Fery-Forgues, S. C. R. *Chimie* **2006**, *9*, 1252–1259.
(27) Uchiyama, S.; Takehira, K.; Yoshihara, T.; Tobita, S.; Ohwada, T. *Org. Lett.* **2006**, *8*, 5869–5872.
(28) Christie, R. M.; Morgan, K. M.; Islam, M. S. *Dyes Pigm.* **2008**, *76*, 741–747.
(29) Luo, X.; Naiyun, X.; Cheng, L.; Huang, D. *Dyes Pigm.* **2001**, *51*, 153–159.
(30) Peng, M.-S.; Cai, J. *Dyes Pigm.* **2008**, *79*, 270–272.
(31) Wang, J.; Qian, X.; Cui, J. *J. Org. Chem.* **2006**, *71*, 4308–4311.
(32) Lin, W.; Yuan, L.; Feng, J.; Cao, X. *Eur. J. Org. Chem.* **2008**, *73*, 2689–2692.
(33) Lim, N. C.; Schuster, J. V.; Porto, M. C.; Tanudra, M. A.; Yao, L.; Freake, H. C.; Bruckner, C. *Inorg. Chem.* **2005**, *44*, 2018–2030.
(34) Ma, Y.; Luo, W.; Quinn, P. J.; Liu, Z.; Hider, R. C. *J. Med. Chem.* **2004**, *47*, 6349–6362.
(35) Lee, M.-T.; Yen, C.-K.; Yang, W.-P.; Chen, H.-H.; Liao, C.-H.; Tsai, C.-H.; Chen, C. H. *Org. Lett.* **2004**, *6*, 1241–1244.
(36) Swanson, S. A.; Wallraff, G. M.; Chen, J. P.; Zhang, W.; Bozano, L. D.; Carter, K. R.; Salem, J. R.; Villa, R.; Campbell, S. *Chem. Mater.* **2003**, *15*, 2305–2312.
(37) Panchuk-Voloshina, N.; Haugland, R. P.; Bishop-Stewart, J.; Bhalgat, M. K.; Millard, P. J.; Mao, F.; Leung, W.-L.; Haugland, R. P. *J. Histochem. Cytochem.* **1999**, *47*, 1179–1188.
(38) Brun, M.-P.; Bischoff, L.; Garbay, C. *Angew. Chem., Int. Ed.* **2004**, *43*, 3432–3436.
(39) Zhao, Y.; Zheng, Q.; Dakin, K.; Xu, K.; Martinez, M. L.; Li, W.-H. *J. Am. Chem. Soc.* **2004**, *126*, 4653–4663.
(40) Eckardt, T.; Hagen, V.; Schade, B.; Schmidt, R.; Schweitzer, C.; Bendig, J. *J. Org. Chem.* **2002**, *67*, 703–710.
(41) Coleman, R. S.; Berg, M. A.; Murphy, C. J. *Tetrahedron* **2007**, *63*, 3450–3456.
(42) Kim, H. M.; Fang, X. Z.; Yang, P. R.; Yi, J.-S.; Ko, Y. G.; Piao, M. J.; Chung, Y. D.; Park, Y. W.; Jeon, S.-J.; Cho, B. R. *Tetrahedron Lett.* **2007**, *48*, 2791–2795.
(43) Dillingham, M. S.; Tibbles, K. L.; Hunter, J. L.; Bell, J. C.; Kowalczykowski, S. C.; Webb, M. R. *Biophys. J.* **2008**, *95*, 3330–3339.
(44) Webb, M. R.; Corrie, J. E. T. *Biophys. J.* **2001**, *81*, 1562–1569.
(45) Katritzky, A. R.; Cusido, J.; Narindoshvili, T. *Bioconjugate Chem.* **2008**, *19*, 1471–1475.
(46) Komatsu, K.; Urano, Y.; Kojima, H.; Nagano, T. *J. Am. Chem. Soc.* **2007**, *129*, 13447–13454.
(47) Komatsu, H.; Miki, T.; Citterio, D.; Kubota, T.; Shindo, Y.; Kitamura, Y.; Oka, K.; Suzuki, K. *J. Am. Chem. Soc.* **2005**, *127*, 10798–10799.
(48) Webb, W. R.; Corrie, J. E. T. *Biophys. J.* **2001**, *81*, 1562–1569.
(49) Suppan, P.; Ghoneim, N. *Solvatochromism*; The Royal Society of Chemistry, Cambridge, U.K., 1997; ISBN 0-85404-419-1.

Table 1. Calculated and Measured Maximum Absorption Wavelengths of **1a**−**g**

Coumarin	Structure	λ_{max}[a]	λ_{max}[b]	λ_{max}[c]
1a	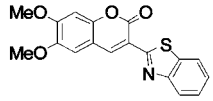	393 (.98)	-	405
1b	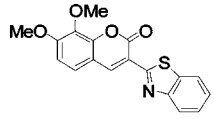	387 (.92)	-	386.5
1c	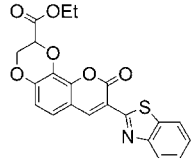	390 (.91)	-	386.5
1d	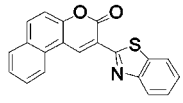	417 (.78)	-	406.5
1e	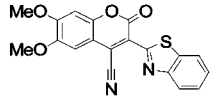	470 (.74)	459 (.74)	455.5
1f	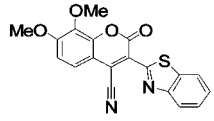	467 (.71)	457 (.70)	426
1g	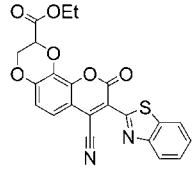	473 (.58) 423 (.16)	462 (.55) 418 (.17)	424

[a] Planar geometry, calculated by time-dependent DFT (B3LYP/6-31G*>), PCM acetonitrile. Values in parentheses indicate the oscillator strength; [b] Twisted geometry, optimized by Hartree−Fock method, optical values calculated by time-dependent DFT (B3LYP/6-31G*). Values in parentheses indicate the oscillator strength. [c] Experimental, solvent: acetonitrile.

patterns onto the basic coumarin rings as well as to put in evidence the differences in the spectroscopic properties of these structures. The performance of DFT methods on coumarins has been already tested.[50,51] For structure optimization we also compared the DFT results with those obtained by the Hartree−Fock method, because DFT has been reported to artificially predict planar structures in molecules where the rotational energy barriers are low.[52] All calculations were performed with the Gaussian 03 package.[53]

The whole set of screened structures is reported in Scheme 1 in Supporting Information.

Our attention was eventually attracted by seven different compounds carrying dialkyl or naphthyl groups in position 6−8, benzothiazene in position 3, and cyano groups in position 4 of the coumarin ring. Indeed, the benzothiazenyl group was predicted to generate a large red-shift of the excitation wavelength, owing to both the extension of the electronic conjugation and the electron-withdrawing effect of the added aromatic ring. Additionally, disubstituted coumarins seem very promising in terms of further functionalization to yield activated "probes" for conjugation to proteins and other biomolecules.

Both DFT/B3LYP and Hartree−Fock revealed that all non-cyano compounds share a planar conformation where the sulfur of benzothiazene and the ring carboxyl group of coumarin are arranged on the same side (the other conformation, where they

(50) Preat, J.; Jacquemin, D.; Perpete, E. A. *Chem. Phys. Lett.* **2005**, *415*, 20–24.
(51) Xu, B.; Yang, J.; Jiang, X.; Wang, Y.; Sun, H.; Yin, J. *J. Mol. Struct.* **2009**, *917*, 15–20.
(52) Zhao, K.; Ferrighi, L.; Frediani, L.; Wang, C.-K.; Luo, Y. *J. Chem. Phys.* **2007**, *126*, 204509–204515.
(53) Frisch, M. J. et al. *Gaussian 03*, Revision B.03; Gaussian, Inc.: Wallingford, CT, 2004.

Scheme 1. Synthesis of **3c**

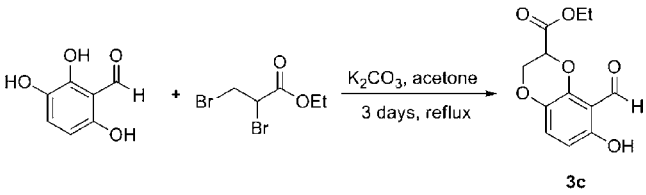

3c

are opposite, is 4−5 kcal/mol higher in energy). In contrast, Hartree−Fock, but not B3LYP, predicted a twisted geometry with an angle of 20−30° between the planes of the coumarin and the benzothiazene rings for the cyano compounds.

The excitation wavelengths and the oscillator strengths calculated by time-dependent DFT (B3LYP/6-31G*) for the planar and the twisted geometries (the latter case only for cyano coumarins) are reported in Table 1. The values are calculated including implicit solvent effects via the polarizable continuum field method (PCM)[54] using acetonitrile as reference solvent with high dielectric constant. The DFT analysis shows a quite strong transition, mainly of $\pi-\pi^*$ character, for all compounds. Excitation wavelengths range in the 390−420 nm and 460−470 nm regions for compounds without and with cyano groups, respectively. Hence, the presence of electron-donating/withdrawing groups red-shifts the $\pi-\pi^*$ transition by 70−180 nm compared to the basic coumarin ring (310 nm). For **1g** DFT predicts additional peaks in the >400 nm region due to excitation to higher excited states.

Apparently, the substitution regioselectivity plays a minor role in determining the transition wavelength. A small red-shift is also associated with the addition of a further aromatic ring compared to alkylether/hydroxyl groups (Table 1, **1a** and **1d**). Notably, the twisted geometry leads to higher transition energies (i.e., shorter wavelengths). This trend was verified also for larger angles (50−90°) between the two aromatic rings, although these were predicted to be higher in energy (∼3 kcal/mol).

2.2. Synthesis of Coumarin Compounds. The first step in our synthetic strategy concerned the synthesis of ethyl 2-(benzo-[*d*]thiazol-2-yl)-acetate **2** starting from the *o*-aminothiophenol and ethyl cyanoacetate. The reaction was carried out under solvent-free conditions at 120 °C to ensure complete conversion to the desired product.[55] **2** played the role of the first reactant in the piperidine-catalyzed Knoevenagel condensation that we designed and accomplished to obtain the final coumarins (Scheme 2).[56]

The other reactants were substituted *o*-hydroxy aldehydes bearing different functional groups (**3a**,**b′**,**c**,**d**). Notably, the two noncommercial hydroxy aldehydes **3a** and **3c** were synthesized through a Vilsmeier formylation reaction and an alkylation by ethyl 2,3-dibromopropionate under basic conditions (Scheme 1), respectively. The Knoevenagel condensation was found to proceed smoothly, and the products (**1a**,**c**,**d**, and **4**) were recovered in excellent yields by simple filtration of the reaction mixture.

4 was further chemically modified in order to complete the toolbox of coumarin chromophores. **1b** was prepared by direct methylation of **4** in nearly quantitative yield. Finally, a cyano group was introduced in position 4 of coumarin **1a**−**c** by an addition/elimination reaction similar to that described in ref 23 (Scheme 2). The latter synthetic path led to the cyano coumarins **1e**−**g** with yields around 80%. Coumarins **1a**−**g** were analytically pure (>99%), as evidenced by HPLC analyses.

Scheme 2. Synthesis of Coumarins; Substituents: $R_1 = R_4 = H$, $R_2 = R_3 =$ OMe (**a**,**e**); $R_1 = R_2 = H$, $R_3 = R_4 =$ OMe (**b,f**); $R_1 = R_2 = H$, R_3,$R_4 = -O\text{-}CH_2\text{-}CH(COOEt)\text{-}O$-(**c,g**); R_1,R_2 = fused phenyl ring, $R_3 = R_4 = H$ (**d**); $R_1 = R_2 = H$, $R_3 = R_4 =$ OH (**4**)

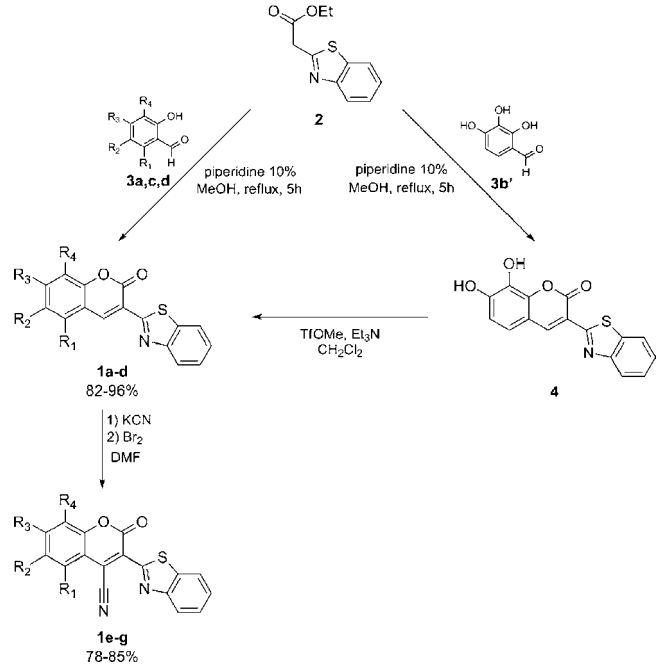

2.3. General Optical Properties of the Coumarin Compounds. Absorption and fluorescence spectra in acetonitrile contain all the principal optical features of the prepared coumarins found also in other solvents and need to be described first. Furthermore, acetonitrile data allow for a comparison with spectroscopic characteristics determined by DFT. The absorption and excitation/emission spectra of representative compounds **1a**, **1c**, **1d** and **1e** are shown in Figure 1, whereas quantitative data can be found in Table 2.

The absorption maxima of coumarins devoid of the cyano group were found to be in excellent agreement with the theoretical values (Table 1). These compounds showed large absorption bands (in some cases also retaining vibrational substructure) peaking in the 380−410 nm interval (Figure 1a−c). Furthermore, these compounds were found to possess broad fluorescence emission spectra spanning 400−600 nm (Figure 1), associated with remarkably high fluorescence quantum yields (Table 2). Excitation spectra were superimposable on absorption spectra, indicating that the quantum yield is independent of the excitation wavelength (data not shown).

Comparison of **1a** and **1d** (Figure 1a,c) suggests that two methoxy groups (**1a**) or a further aromatic ring (**1d**) have approximately the same electronic effect on both the fundamental and excited states on account of a substantial constancy of absorption and emission wavelengths. Instead, the transfer of a methoxy group from position 6 to 8 on the coumarin ring leads to 10−20 nm blue-shifts of absorption and emission maxima (Table 2, compare **1a** and **1b**). Substitution of two methoxy groups with one bidentate alkyl ether amenable to further functionalization affects neither the absorption nor the emission properties of the molecule (Table 2, compare **1b** and **1c**).

(54) Cossi, M.; Barone, V. *J. Chem. Phys.* **2001**, *115*, 4708–4718.
(55) Abbotto, A.; Bradamante, S.; Facchetti, A.; Pagani, G. A. *J. Org. Chem.* **2002**, *67*, 5753–5772.
(56) Lee, S.; Sivakumar, K.; Shin, W.-S.; Xie, F.; Wang, Q. *Bioorg. Med. Chem. Lett.* **2006**, *16*, 4596–4599.

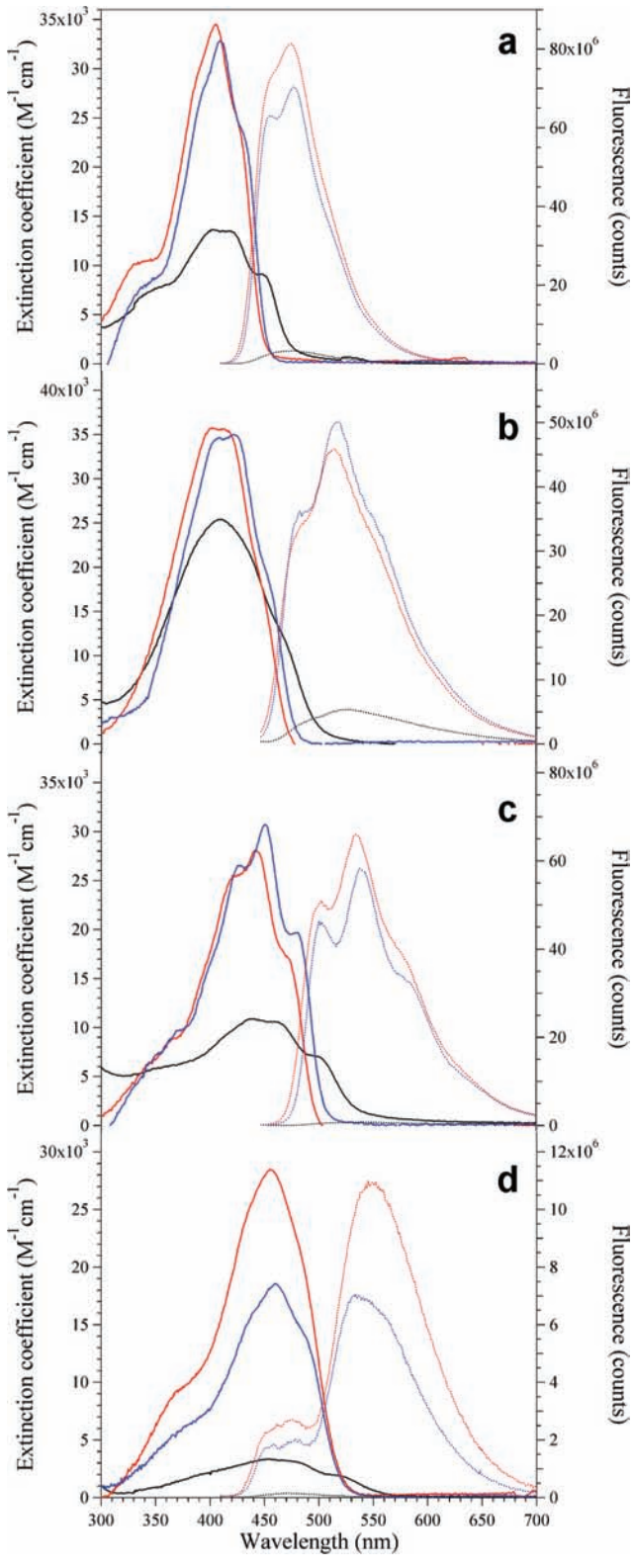

Figure 1. Absorption (full line) and emission (dotted line, $\lambda_{exc} = 405$ nm) spectra in water (black), acetonitrile (red), and 1-octanol (blue) of coumarins **1a** (a), **1c** (b), **1d** (c), **1e** (d).

As expected, the introduction of a cyano group in position 4 of the ring leads to a significant absorption and emission red-shift (Table 2, Figure 1d). **1e** is characterized by easily detected dual fluorescence emission (Figure 1d). Selective excitation at the absorption maxima is associated with a unique broad emission peak at 550 nm and covering the 480−700 nm interval. Conversely, excitation of the high-energy absorption shoulder (<370 nm) leads always to a composite emission spectra encompassing two bands in nearly fixed intensity ratio: the first band peaks at 470 nm (λ_{sh}), and the second is identical to that obtained by excitation at absorption maximum. Importantly, this spectroscopic pattern, and particularly the invariant intensity ratio between the two bands, was found to be independent of fluorophore concentration, thus ruling out the formation of excimers (Supporting Information). We shall provide a more detailed explanation of these features in the Discussion section.

Table 2. Spectroscopic Data of Compounds **1a**−**g**

	H_2O	*i*-PrOH	H_2O/*i*-PrOH	DMSO	ACN	OctOH	AcOEt	Diox	H_2O/Diox
1a									
λ_{max}	401.5	407	409.5	411	405	409.5	405.5	406	408.5
ε^a	1.3	3.6	3.8	3.5	3.4	3.3	3.5	3.9	3.3
λ_{em}	475	475	476	480	474	477	472	473	478
Φ^b	0.10	0.88	0.86	0.95	0.86	0.89	0.88	0.86	0.84
1b									
λ_{max}	381.0	389.5	393	393	386.5	392.5	387.5	387	389
ε^a	0.4	3.7	3.6	3.7	3.7	3.6	4.5	4.1	4.3
λ_{em}	487	465	470	471	464	466	460	461	470
Φ^b	0.01	0.74	0.65	0.78	0.86	0.75	0.79	0.78	0.55
1c									
λ_{max}	382	388.5	389.5	392	386.5	391.5	387	387	389
ε^a	2.5	4.4	4.1	3.9	3.6	3.5	3.8	4.1	4.6
λ_{em}	470	461	466	468	460	463	457	458	466
Φ^b	0.12	0.81	0.75	0.82	0.81	0.86	0.85	0.85	0.72
1d									
λ_{max}	403.5	411	414	413.5	406.5	413	407.5	408	412.5
ε^a	1.0	2.8	1.9	2.8	2.8	3.1	3.3	3.3	2.7
λ_{em}	481	478	482	486	476	479	474	484	475
Φ^b	0.04	0.89	0.92	0.86	0.87	0.87	0.83	0.83	0.86
1e									
λ_{max}	454.5	457.5	461	461.5	455.5	460	455.5	454.5	458.5
ε^a	0.3	1.6	1.8	2.6	2.8	1.8	3.3	3.0	1.8
λ_{em}	581	541	558	560	549	539	534	526	560
Φ^b	0.01	0.40	0.20	0.26	0.41	0.51	0.52	0.59	0.22
λ_{sh}	471	475	476	480	474	478	473	475	478
1f									
λ_{max}	438	428	433	430	426	433	424	424	428
ε^a	0.9	2.7	2.2	2.4	3.3	2.4	2.2	2.8	2.1
λ_{em}	nd	521	nd	526	nd	529	546	526	nd
Φ^b	<0.01	0.01	<0.01	0.02	<0.01	0.02	0.01	0.02	<0.01
1g									
λ_{max}	430	427	431	427	424	432	424	423	429
ε^a	1.1	2.2	1.5	1.4	2.0	2.1	2.0	2.3	1.7
λ_{em}	555	518	529	520	nd	513	516	507	535
Φ^b	0.01	0.04	0.02	0.02	<0.01	0.1	0.09	0.14	0.01

[a] Molar extinction coefficient ($\times 10^{-4}$). [b] Fluorescence quantum yield.

Cyanocoumarins **1f**,**g** display very poor quantum yields in acetonitrile and in all other solvents (Table 2). Notably, DFT calculations overestimated the actual absorption wavelength of these cyanocoumarins (Tables 1 and 2). On account of the calculated dependence of transition energy on the twist angle between the two aromatic rings, this discrepancy may arise from more distorted geometry than predicted by our theoretical analysis. This condition could be at basis of the observed poor emissivity, assuming that a distorted conformation promotes nonradiative decay channels.

2.4. Solvatochromic Properties of the Coumarin Compounds. Next, we set out to investigate the solvatochromic behavior of compounds **1a**−**g**. For this goal, we measured absorption and fluorescence spectra at 25 °C in an ensemble of solvents covering a large polarity interval as expressed by the orientation

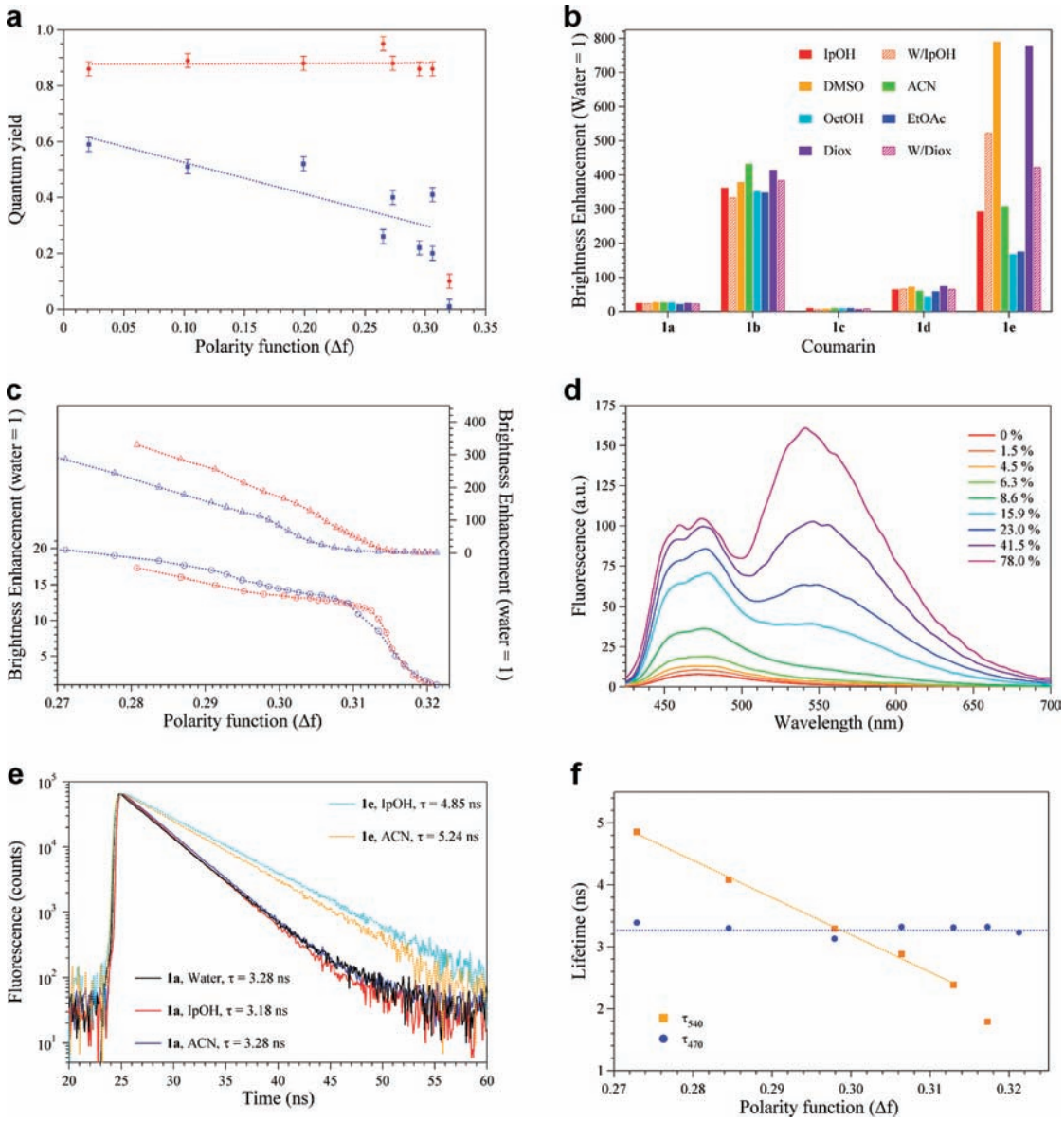

Figure 2. (a) Polarity dependence of emission quantum yield for **1a** (red) and **1e** (blue). (b) Relative brightness (absorption × quantum yield) enhancement (Water = 1) for coumarins **1a**−**e**. (c) Brightness enhancement for **1a** (bottom) and **1e** (top) in water/*i*-PrOH (red) and water/Dioxane (blue) mixtures. (d) Fluorescence emission of **1e** upon excitation at 405 nm in different mixtures water/*i*-PrOH (v/v percentages of isopropanol are indicated in the legend). (e) Fluorescence lifetimes of **1a** (λ_{exc}: 403 nm) and **1e** (λ_{exc}: 468 nm) in water, *i*-PrOH, and acetonitrile. (f) Polarity-dependence of fluorescence lifetimes of **1e** upon excitations at 403 nm (blue) and 468 nm (orange).

polarizability Δf:[57,58] water (symbol: W, $\Delta f = 0.32$), acetonitrile (ACN, $\Delta f = 0.306$), isopropanol (*i*-PrOH, $\Delta f = 0.273$), dimethylsulfoxide (DMSO, $\Delta f = 0.265$), ethyl acetate (EtOAc, $\Delta f = 0.199$), *n*-octanol (OctOH, $\Delta f = 0.103$), and 1,4-dioxane (Diox, $\Delta f = 0.021$). 50/50 vol % mixtures of W/*i*-PrOH ($\Delta f = 0.306$) and W/Diox ($\Delta f = 0.295$) were also added to provide media with intermediate hydrogen-bonding capabilities. Very apolar solvents such as *n*-hexane were avoided, as the coumarins became rather insoluble. Spectroscopic data for the coumarins in all solvents are reported in Table 2.

On one hand, all coumarins display high extinction coefficients and quantum yields in organic solvents or water/solvent mixtures, resulting in bright fluorescence (Table 2, Figure 1). On the other hand, fluorescence emission of all compounds is nearly abolished in water, as witnessed by the very low quantum yields and lower extinction coefficients measured in this medium (Table 2, Figure 1). Remarkably, quantum yields of non-cyanocoumarins **1a**−**d** do not correlate with the polarity function (Δf), being rather constant in organic or water/organic media and much lower in water (Figure 2a, red). A somewhat stronger correlation between quantum yield and Δf is observable for the fluorescent cyanocoumarin **1e** (Figure 2a, blue). All coumarins, however, displayed no correlation at all between absorption (or emission) wavelength and Δf. As such a correlation would be expected by the classical Lippert−Mataga's theory of solvatochromism, these findings suggest a specific interaction between water molecules and the coumarin structures that strongly perturbs the photophysical behavior of the latter ones. The band broadening of the absorption spectra in water is a further support to this hypothesis.

(57) Suppan, P. *J. Chem. Soc. A* **1968**, 3125–3133.
(58) Weast, R. C. *Handbook of Chemistry and Physics*; CRC Press: Boca Raton, FL, 1980.

The fluorophore brightness (i.e., the product of extinction coefficient and quantum yield) is a parameter immediately associated with the fluorescence emission performance in environments of different polarity at constant excitation power, as typically occurring in cell imaging. Accordingly, we computed the absolute brightness (Supporting Information, Table S1) and water-relative brightness (Figure 2b) of our coumarins. Among non-cyanocoumarins, **1b** displays an astonishing >350-fold increment of brightness going from water to water/organic or organic media. Nonetheless, **1a** is associated with the highest absolute brightness in non-water solvents (>28,000, Supporting Information, Table S1). Cyanocoumarin **1e** shows a quite variable water-relative brightness (between 170−790), in keeping with its more solvent-modulated extinction coefficient and quantum yield.

To determine the pattern of change in brightness between water and organic media, we measured the water-relative brightness of **1a** and **1e** in W/*i*-PrOH and W/Diox mixtures characterized by different Δf values (Figure 2c). For both mixtures, the relative brightness of **1a** displays a rapid increase for Δf above ~0.31, whereas it follows a slower linear trend for $\Delta f <$ ~0.31. More precisely, the linear phase begins below $\Delta f = 0.312$ (10% mol) for W/*i*-PrOH or $\Delta f = 0.309$ (7% mol) for W/Diox. Thermodynamic studies on W/IpOH or W/Diox mixtures have shown that at low molar content of organic solvent (5−10% in mol), water undergoes a transition to structure II "clathrates", which are characterized by an ice-like arrangement of 136 H_2O molecules to give 24 cavities. Eight of these cavities are large enough to accommodate guest molecules such as the organic solvent, whereas the other are smaller and should contain "monomeric" H_2O molecules (i.e., not hydrogen-bonded with the infinite network).[59] At higher *i*-PrOH or Diox content, small clusters of organic solvent and water molecules are formed.[60] These findings prompt us to attribute the sharp variation of brightness of **1a** to the structural rearrangement of water that leads presumably to the loss of several H-bonds established with surrounding H_2O molecules. The linear trend at higher organic content may be related to a more "classical" solvatochromic effect.

Significantly, in both W/*i*-PrOH and W/Diox compound **1e** shows low and constant brightness in the same Δf range where its non-cyano counterpart **1a** experiences a sharp increase of emission. Below this region, brightness of **1e** is linearly related to polarity. This trend suggests that **1e** cannot fluoresce in the whole region of clathrate stability, becoming emissive only when the water molecules become more "monomeric" and surrounded by their organic counterparts. **1e** is associated with a further peculiar photophysical property: its dual fluorescence upon high-energy excitation (below 405 nm) appears in all organic solvents, and for water/organic mixtures, it is dependent on the organic content (Figure 2d). In fact, both the high-energy (470 nm) and the low-energy (540 nm) emission bands increase as the water content of the mixture is decreased. The low-energy band ($\lambda =$ 550 nm) is more sensitive to the polarity of the mixture than its high-energy companion ($\lambda_{sh} = 470$ nm). The latter one never disappears, even in pure water. Thus, the ratio between the two bands changes with the polarity of the mixture. This behavior supports the use of **1e** as a ratiometric (i.e., concentration independent)[61] sensor of medium polarity.

Table 3. Fluorescence Lifetimes of **1a**,**c**,**e** in Water, Isopropanol, and Acetonitrile; Intrinsic Lifetime Values Calculated from the Strickler−Berg Relation[62] are Reported in Parentheses

	fluorescence lifetime (ns)			radiative lifetime (ns)		
coumarin	H_2O	*i*-PrOH	CAN	H_2O	*i*-PrOH	ACN
1a	3.28	3.18	3.28	32.8 (6.62)	3.6 (3.13)	3.8 (3.19)
1c	2.44	2.69	2.65	20.3 (4.03)	3.32 (2.52)	3.27 (3.03)
1e	3.23	4.85	5.24	323.0 (36.2)	12.1 (8.28)	12.8 (5.29)

2.5. Fluorescence Lifetime Measurements. On account of their non-negligible fluorescence in water, coumarin **1a**,**c** were selected to test the effect of solvent nature on the fluorescent lifetime (τ). **1e** was added to this pool to compare the photophysical characteristics after the incorporation of the cyano group. Actually, as already mentioned, **1e** displays dim but detectable fluorescence in water when excited at 405 nm.

Remarkably, **1a**,**c**,**e** are all characterized by monoexponential decays when excited near their absorption maximum (403 nm for **1a**,**c**, 468 nm for **1e**) regardless of the solvent (Figure 2e). Lifetime values range from 2.8 to 5.24 ns (Table 3). The actual lifetimes can be combined with the quantum yields to give the corresponding radiative lifetimes (τ_r, Table 3).

For **1a**,**c**, the position and nature of the functional groups attached to the coumarin ring modulate the detected lifetime. Interestingly, for both coumarins τ is quite constant in the three tested solvents, whereas τ_r becomes extremely large (>30 ns) in water. The theoretical τ_r in water calculated by the Strickler−Berg equation from the absorption and fluorescence spectra is around 3 ns, an order of magnitude lower than the experimental value. Instead, the theoretical τ_r in *i*-PrOH and ACN are in good agreement with the experimental value (Table 3). The Strickler−Berg equation fails to yield reasonable values of τ_r only when a strong interaction with the solvent takes place and/or there is a change in the excited-state geometry. These data suggest that the low quantum yields of **1a**,**c** in water are not the result of some quenching process but rather of different properties of the excited state. A photophysical model accounting for this phenomenology will be described in the Discussion section.

The cyano group in **1e** leads to significantly longer τ and τ_r (Table 3). Here, τ_r is significantly larger than the theoretical value in all media, suggesting efficient interactions between the molecule and the selected solvents. We further examined the effect of medium polarity on the lifetime of **1e** by collecting measurements in W/*i*-PrOH mixtures at different Δf (Figure 2f, orange trace). Notably, the τ values show remarkable linearity with Δf up to 0.315, in good agreement with the brightness behavior in the W/*i*-PrOH media (Figure 2c). These data confirm that the fluorescence of **1e** is regulated by a "classical" solvatochromic behavior once the water content falls below a threshold value (around 90% in mol). We also determined the τ values of **1e** upon 403-nm excitation in the same W/*i*-PrOH mixtures in order to check the effect of the dual fluorescence emission. Indeed, we always collected biexponential fluorescence decay curves except for the pure water case. To determine the actual τ values of the high-energy emission component (τ_{470}),

(59) Jerie, K.; Baranowski, A.; Koziol, S.; Glinski, J.; Burakowski, A. *Chem. Phys.* **2005**, *309*, 277–282.
(60) Østergaard, K. K.; Tohidi, B.; Anderson, R.; Todd, A. C.; Danesh, A. *Ind. Eng. Chem. Res.* **2002**, *41*, 2064–2068.
(61) Bizzarri, R.; Serresi, M.; Luin, S.; Beltram, F. *Anal. Bioanal. Chem.* **2009**, *393*, 1107–1122.
(62) Valeur, B. *Molecular Fluorescence*; Wiley-VCH Verlag GmbH: Weinheim (DE), 2002.

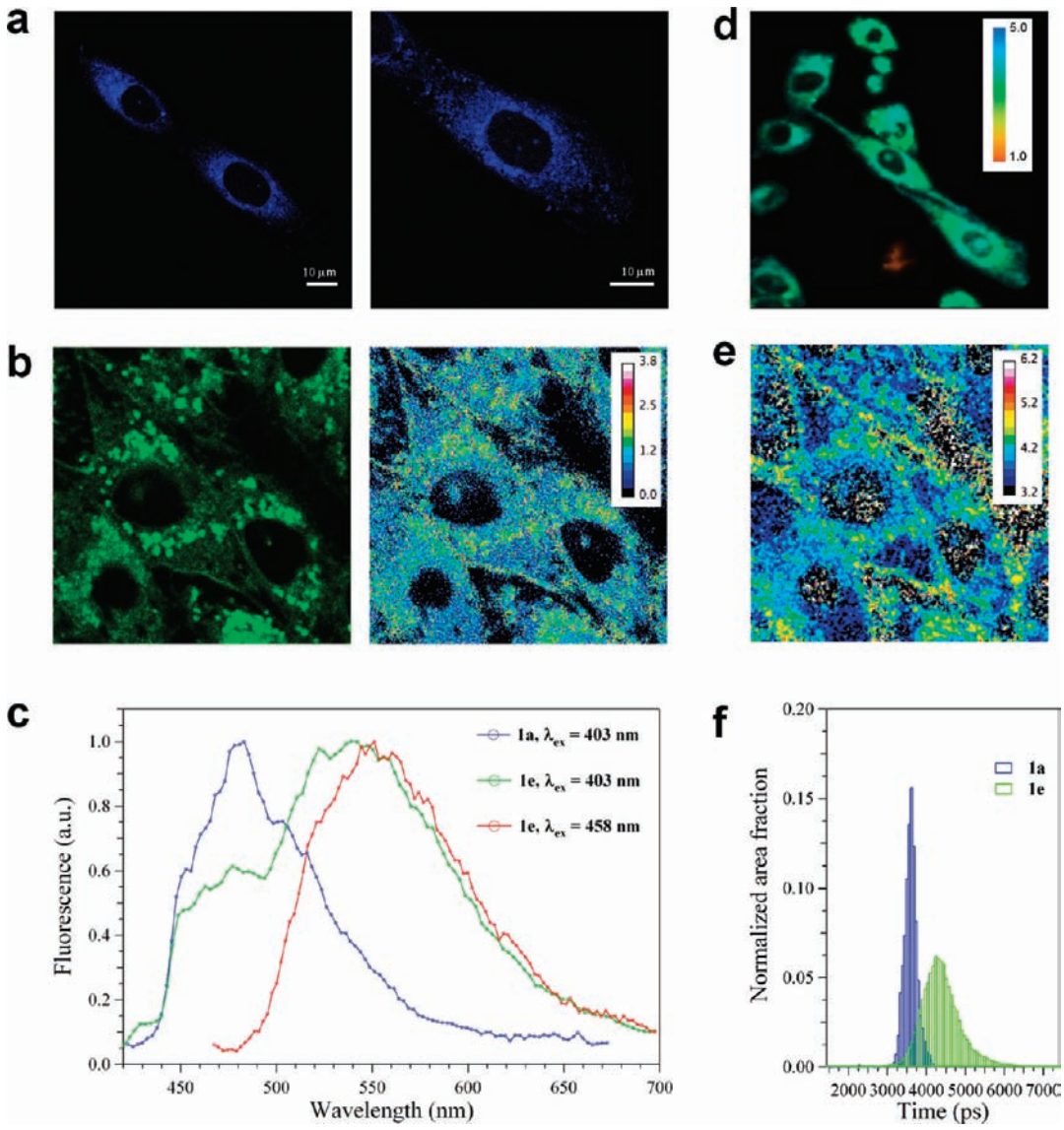

Figure 3. (a) Confocal microscopy images of **1a** in CHO cells (λ_{exc}: 403 nm). (b) (Left) Confocal microscopy image of **1e** in CHO cells (λ_{exc} = 403 nm, λ_{em} = 545−580 nm). (Right) Ratio of images collected at 545−580 nm and 440−480 nm (λ_{exc} = 403 nm). (c) Fluorescence spectra of **1a** and **1e** in CHO cells. (d) Lifetime-intensity color-coded map of **1a** in CHO cells (λ_{exc}: 403 nm). (e) Color-coded lifetime map of the image reported in panel b (λ_{exc} = 468 nm). (f) Histogram of lifetime distribution for **1a** and **1e** in CHO cells.

we fitted the biexponential decays imposing one lifetime equal to that recovered by excitation at 468 nm. Importantly, we found that λ_{470} is almost invariant with solvent polarity (Figure 2f, blue trace) and its value (3.30 ns) is very close to its non-cyano counterpart **1a**.

2.6. Photophysical Properties in Cultured Cells. In order to assess the photophysical behavior of the prepared coumarins in biological environments, compounds **1a**−**e** were examined in living cells. The dyes were externally administered at low concentration (0.5−1 μM) to Chinese Hamster Ovary (CHO) cell cultures. After 15−30 min of exposition, cells were imaged by a confocal microscope without removing the external buffer by using 403 nm and/or 458 nm excitation laser source (Figure 3a,b).

CHO cells remained viable for at least 2−3 h after addition of the coumarins. No fluorescence was detected in the external buffer, or in the nucleus, while collected images showed that the coumarins are emissive in selected lipophilic subcellular compartments. These findings are in agreement with the negligible fluorescence of **1a** and **1e** in water, as well as the rather lipophilic properties of the dyes.

Remarkably, the emission profiles of the coumarins in the subcellular region where they are active (Figure 3c) resemble closely those determined during *in vitro* experiments, indicating that the biological environment does not affect the fluorescent optical characteristics of the coumarins. The conserved dual emission of **1e** upon high energy (403 nm) excitation (Figure 3c) is particularly relevant in view of the use of this coumarin as ratiometric emission indicator of polarity, working in the visible region of the spectrum. A ratiometric plot of polarity by **1e** is reported in Figure 3b (right) and compared with the lifetime map (Figure 3e) to which it is strictly related (see below).

The lifetimes of **1a** and **1e** were analyzed in cultured cells by confocal FLIM. **1a** was found to possess a quite uniform monoexponential lifetime decay cell-wide (Figure 3d,f), in excellent agreement with its constant lifetime observed in medium of different polarity *in vitro*. Also the intracellular

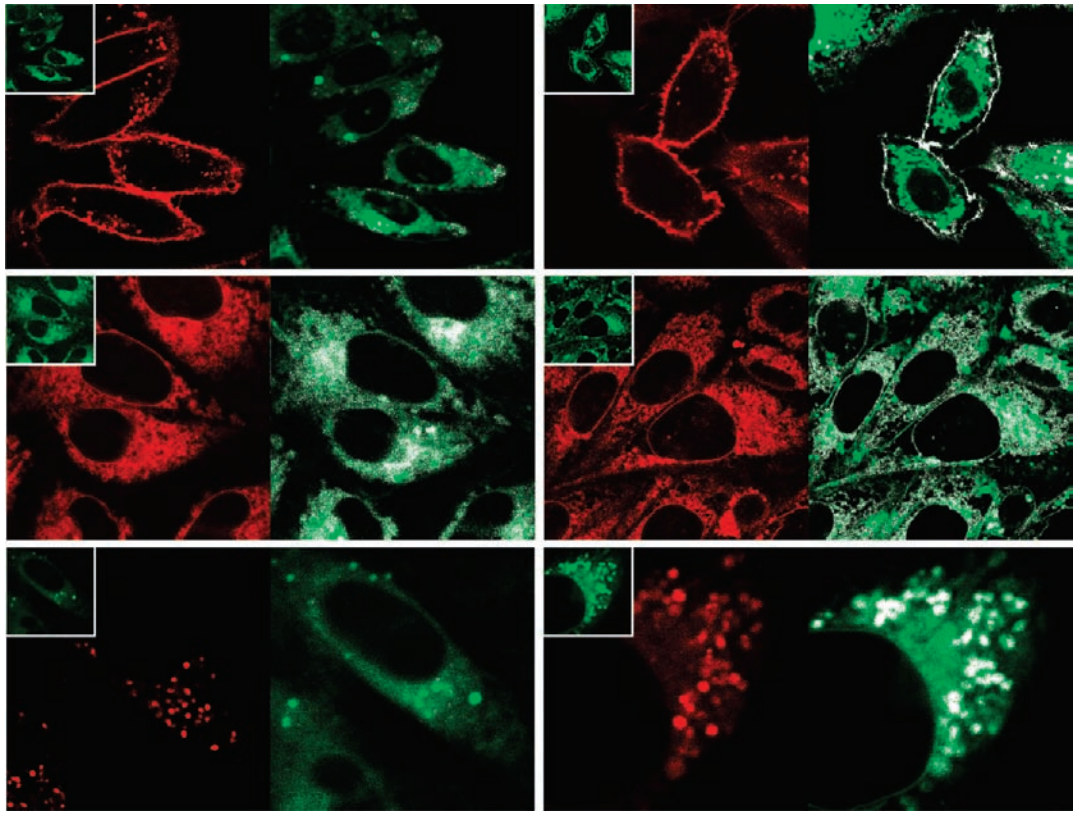

Figure 4. Colocalization of standard organelle markers (left, red channel) and **1a** or **1e** (right, green channel, and inset) in CHO cells. White spots represent a selection of colocalized points (intensity ratio interval: 0.85−1.17). Colocalization results, obtained by a colocalization P-test according to Fay's method[64] are reported in parenteses. (a) **1a** (λ_{exc}: 403 nm, λ_{em} = 420−600 nm) and membrane marker DiIC18(5)-DS (λ_{exc}: 633 nm, λ_{em} = 650−750 nm) (poor colocalization, $P = 0.46$); (b) **1a** (λ_{exc}: 458 nm, λ_{em} = 470−550 nm) and ER marker BODIPY TR glibenclamide (λ_{exc}: 561 nm, λ_{em} = 570−680 nm) (strong colocalization, $P > 0.95$); (c) **1a** (λ_{exc}: 403 nm, λ_{em} = 410−535 nm) and lysosome marker Lysotracker (λ_{exc}: 561 nm, λ_{em} = 570−700 nm) (moderate colocalization, $P = 0.68$); (d) **1e** (λ_{exc}: 458 nm, λ_{em} = 470−600 nm) and membrane marker DiIC18(5)-DS (λ_{exc}: 633 nm, λ_{em} = 650−750 nm) (strong colocalization, $P > 0.95$); (e) **1e** (λ_{exc}: 458 nm, λ_{em} = 470−600 nm) and ER marker BODIPY TR glibenclamide (λ_{exc}: 561 nm, λ_{em} = 570−680 nm) (strong colocalization, $P > 0.95$); (f) **1e** (λ_{exc}: 458 nm, λ_{em} = 470−600 nm) and lysosome marker Lysotracker (λ_{exc}: 561 nm, λ_{em} = 570−700 nm) (strong colocalization, $P > 0.95$). Note that in experiments involving **1e** the two dyes were imaged sequentially to avoid extensive cross-talk.

lifetime behavior of **1e** was in keeping with the properties measured *in vitro*. Upon 468 nm excitation, we detected monoexponential decays with τ fairly dependent on the intracellular location. Careful analysis showed that longer lifetimes were associated with **1e** localized in cell membranes or the perinuclear region, owing to the more lipophilic character of these regions (Figure 3e,f). Additionally, the lifetime map of **1e** is very similar to its emission ratiometric map (Figure 3b,e), i.e. there is a strict correspondence between longer fluorescence lifetimes and increased low-/high-energy band ratio, as previously found *in vitro*. These data highlight the possibility of using **1e** as a gradual polarity indicator in bioenvironments by both emission ratiometry and lifetime imaging.

Finally, the photostability of **1a** and **1e**, measured at high laser power in living cells, was quite comparable with that of YFP. Indeed, we measured fluorescence decrease with $\tau = 39.5 \pm 2$ s (93.1 kW/cm^2), 13.7 ± 0.5 s (135 kW/cm^2), and 30.3 ± 0.8 s (106 kW/cm^2) for YFP, **1a**, and **1e**, respectively.

2.7. Cellular Localization of Coumarins. To gain further insight into the partitioning of **1a** and **1e** within different subcellular domains, we performed some colocalization experiments with standard organelle markers, in particular DiIC18(5)-DS (membrane marker), BODIPY TR glibenclamide (ER marker), and Lysotracker (lysosome marker). We found similar, although not superimposable, localizations of **1a** and **1e**, according to the different physicochemical properties of our probes. **1a** extensively accumulated in ER (Figure 4b), whereas its localization in the cell membrane (Figure 4a), lysosomes (Figure 4c), and Golgi apparatus (not shown) was rather limited. **1e** accumulated in the cell membrane (Figure 4d) and ER (Figure 4e). Also, this coumarin is extensively sequestered in lysosomes (Figure 4f), giving rise to punctate staining (see Figure 3b for comparison). Cell localization differences can be clearly evidenced by a ratio plot of **1a** and **1e** fluorescence taken in cells exposed to both coumarins (Figure 5a−c). These findings suggest a preferential albeit different localization of **1a** and **1e** in lipophilic compartments, in agreement with the hydrophobic coumarin structure. Consistently, we measured log *P* values of 3.6 for **1a** and 2.9 for **1e**,[63] substantiating the hypothesis of a significant accumulation of the dye in the most apolar domains of the cell but with different affinity. The presence of the fluorophore in the cytosol could not be evidenced directly, due to the nonemissivity of the solvatochromic probes in aqueous environment. However, by means of simple fluorescence recovery after photobleaching (FRAP) experiments, we found that the coumarins have remarkably high diffusivity throughout the cell ($\tau = 3.1 \pm 0.6$ s, $\tau = 5.6 \pm 0.5$ s for **1a** and **1e**,

(63) Takács-Novák, K.; Avdeef, A. *J. Pharm. Biomed. Anal.* **1996**, *14*, 1405–1413.
(64) Fay, F. S.; Taneja, K. L.; Shenoy, S.; Lifshitz, L.; Singer, R. H. *Exp. Cell Res.* **1997**, *231*, 27–37.

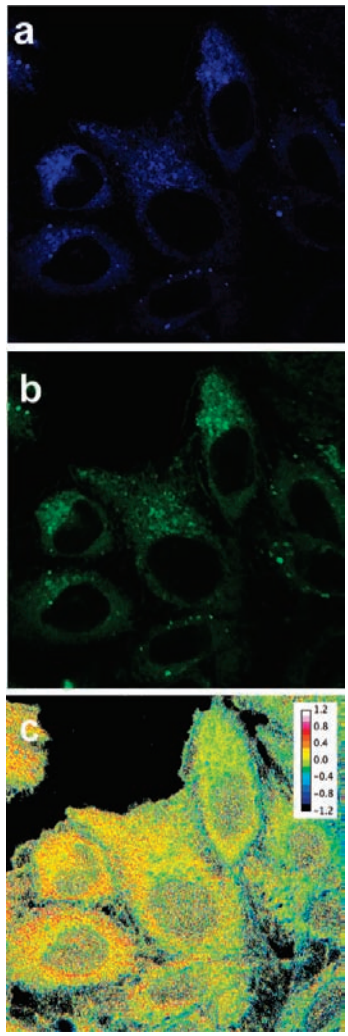

Figure 5. (a,b) Confocal microscopy image of **1a** (panel a, $\lambda_{exc} = 405$ nm, $\lambda_{em} = 420-470$ nm) and **1e** (panel b, $\lambda_{exc} = 458$ nm, $\lambda_{em} = 500-600$ nm), concomitantly administered to CHO cells; (c) logarithm of the ratio of images a and b to unveil different intracellular distributions of **1a** and **1b**; note that the log form was adopted to display spatial enrichment or depletion in linear color-coded scale.

respectively),[5] thus suggesting a partition equilibrium of the dyes between the lipophilic compartments and the cytosol.

3. Discussion

Environmentally sensitive fluorescent molecules appear extremely useful for *in vivo* imaging applications. They can be used as sensors to report on polarity changes in the surrounding medium associated with relevant biochemical events such as protein−protein recognition, membrane lipid restructuring, and biomolecular self-assembly processes. Note that compared to the more popular FRET-based sensors, solvatochromic probes do not require two partners in close proximity and in well-defined geometrical relationships to provide a signal which monitors the target process at nanoscale. Hence, we recently developed a renewed interest in molecular moieties optically influenced by the polarity of their environment.

The solvatochromic behavior usually stems from large variations of the molecular dipole upon photon absorption, leading to different stabilization energies of the ground and excited states by the solvent shell around the molecule. The concomitant incorporation of electron-donating and electron-withdrawing groups onto aromatic rings is a common way to promote solvatochromism. In such a case, the electronic transition is often accompanied by a large transfer of electronic charge from the electron donor toward the electron acceptor, a phenomenon referred to as intramolecular charge transfer (ICT). The significant electron redistribution between ground and excited state upon photoexcitation results in a sudden change of molecular dipole moment and therefore of stabilization by the solvent. Nonetheless, a powerful solvatochromic effect is not necessarily translated into a bright and polarity-dependent fluorescence. Indeed, the addition of donating or withdrawing group to otherwise fluorescent aromatic molecules may forbid or severely hamper the fluorescence emission of the target compound.

The coumarin aromatic structure is known to allow the incorporation of electron donors and acceptors while retaining most of its excellent fluorescent properties such as high quantum yield and large Stokes' shift. In this perspective, we targeted the engineering of a novel toolbox of coumarins bearing different functional groups in a donor−(coumarin core)−acceptor configuration. The attention was mainly directed to alkylether groups as good electron-donating functional units, since they are amenable to further modification to yield chemical "hands" for biomolecule binding. Additionally, alkylether groups prevent the chemical reactivity problems (e.g., protonation, low yield of further functionalization) that are often encountered when the more popular electron-donating amino group is utilized. We focused on benzothiazene and cyano functional units as acceptor groups on account of their reported electron-withdrawing effect on the physicochemical properties of conjugated aromatic compounds.[29] It is worth noting that all these groups were singularly described to red-shift the basic coumarin spectra[23] owing to a larger delocalization of the π orbital.

Our approach to the development of new solvatochromic fluorescent probes followed a sequential scheme: (1) *in silico* screening to identify interesting substitution patterns of the coumarin structure from an optical viewpoint, (2) establishment of a reliable and efficient synthetic procedure common for all the target compounds (modular synthesis), (3) thorough *in vitro* analysis of the photophysical properties of the synthesized probes, and (4) evaluation of their photophysical behavior in a biological (e.g., cultured cell) environment. Overall, we sought to set up a general and flexible scientific "platform" to engineer probes tailored to different *in vivo* applications.

The computational DFT screening of coumarin structures was carried out with the clear-cut goal of identifying donor−(coumarin core)−acceptor patterns able to red-shift the absorption of pure coumarin (310 nm) to the visible region of the electromagnetic spectrum, while retaining a molecular structure amenable to biochemical functionalization. Indeed, the visible region is by far the preferred wavelength interval for the analysis of biological specimens owing to the good compromise of high spatial resolution and low photodamage to cellular structures. Accordingly, most microscope apparatus for *in vivo* imaging are supplied with excitation sources emitting above 400 nm. DFT/B3LYP analysis allowed for the identification of seven interesting structures red-shifted of 70−180 nm compared to base coumarin (Table 1, **1a**−**g**). These structures are characterized by the presence of two alkylether- or one naphthyl-donor group in positions 6−8, one benzothiazene group in position 3, and for a subset, also by a cyano group in position 4. We noticed that the nature of alkyl ether and the substitution regioselectivity at positions 6−8 have little effect on absorption wavelength

(Table 1, **1a**−**c**, **1e**−**g**). Furthermore, DFT highlighted that the concomitant incorporation of both benzothiazene and cyano groups yields a synergistic red-shift effect on absorption (Table 1, **1e**−**g**). These findings appeared promising in light of our modular approach to probes tailored for specific applications and prompted for the synthesis of **1a**−**g**. Note that compound **1c** represents already a "functional" evolution of **1b**, as it can be easily converted into a reactant for protein conjugation (we shall describe this in a forthcoming paper).

Concerning the synthetic step, we set up a general procedure based on a piperidine-catalyzed Knoevenagel reaction involving substituted *o*-hydroxy benzaldehydes (Schemes 1−2, **3a**,**b′**,**c**,**d**) and a benzothiazene acetate derivative (Scheme 2, **2**). The cyano group was then added by a simple addition/elimination reaction. Overall, the synthetic procedure allows obtaining the desired coumarin in high yields just by selecting and preparing the appropriate *o*-hydroxy benzaldehyde reactant. Note that the here-adopted Knoevenagel reaction is known to be unaffected by most functional groups that may be present on the reactants.

The absorption properties of the non-cyanocoumarins in acetonitrile closely resemble those calculated by DFT. A good agreement is seen also for cyano **1e**, whereas DFT overestimated the wavelengths of absorption peaks of **1f**,**g**. We attribute the latter discrepancy to larger distortion of the angle between the two aromatic rings than predicted by the theoretical method. Indeed, our calculation clearly correlates the twist angle with the excitation energy. The absorption bands are in all cases broad and often rich in vibrational substructure. Non-cyanocoumarins can be excited efficiently by light sources in the 380−430 nm range (Figure 1a−c); cyanocoumarins allow for excitation wavelengths as long as 500 nm (Figure 1d). With the exception of **1f**−**g**, the prepared coumarins in acetonitrile showed broad fluorescence emission characterized by large Stokes' shifts (Figure 1a−d) and high quantum yields (Table 2). Both properties are extremely relevant in view of a future use of these compounds for high-resolution imaging as they are at the basis of large signal-to-noise ratio. **1e** displays an interesting property: when excited on the high-energy absorption shoulder below 400 nm it adds a minor emission band peaked at 470 nm to its conventional band peaked at 570 nm. This dual fluorescence is associated with a nearly constant band ratio for any excitation below 400 nm (Supporting Information). We demonstrated, however, that this effect is not the result of excimer formation and must be related to the photophysics of the excited state.

From a solvatochromic viewpoint, we can split the fluorescent coumarins into two subsets, one encompassing the non-cyano derivatives, **1a**−**d**, and the other cyano compound, **1e**. The analysis in solvents, or water/solvent mixtures, of different polarities (measured by the orientation polarizability function Δf) showed clearly that **1a**−**d** are poorly or not emissive in pure water, whereas they maintain approximately the same quantum yield once the polarity falls below a certain value ($\Delta f \approx 0.31$) no matter whether that happens in water/organic solvent mixtures or pure protic/nonprotic organic solvents (Figure 2a,b). Brightness enhancements ranged from 15- to 400-fold with respect to pure water (Figure 2b). The sharp increase in fluorescence is clearly related to a rearrangement of water structure and the concomitant loss of strong H-bonding interactions with the solute probe (Figure 2c).

The H-bonding model helps explain also the different QY in water of **1b** and **1c** in spite of the similar substitution pattern. Indeed, we performed molecular dynamics simulations of these two coumarins embedded in explicit water molecules. The simulations describe how water molecules interact with the solute, during its ground-state dynamics, predicting the formation and stability of hydrogen bonds. By comparing the two coumarins, we observed that only the oxygen atom at position 8 (O8) changes significantly its H-bonding degree between the two molecules. In **1b** we found ∼60% of full H-bonding occupation (i.e., ∼60% of the molecular dynamics snapshots show a configuration where a water oxygen is at a distance <3.5 Å and the O8−hydrogen−water oxygen angle is >150°), whereas in **1c** this value drops to ∼20%. Although these values are just estimates of H-bonding capabilities, the comparison between these two figures clearly indicates that O8 of **1b** establishes much stronger H-bonding interactions with water molecules than O8 of **1c**.

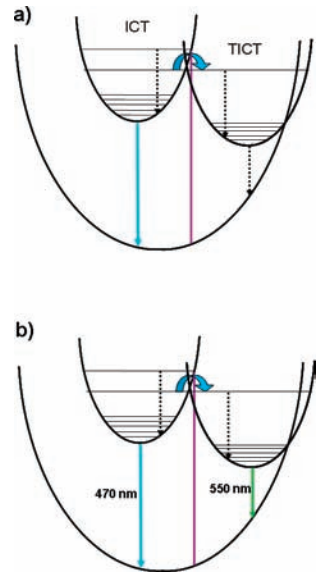

Figure 6. Proposed model of electronic transitions in coumarins **1a**−**d** (a) and **1e** (b).

To further investigate the photophysical behavior of these coumarins we determined the fluorescence lifetimes in water, *i*-PrOH, and ACN of **1a** and **c** (**1b**,**d** are practically nonfluorescent in water, and reliable fluorescence decays could not be obtained). Surprisingly, the lifetime is very similar in these three solvents (Table 3). The radiative lifetime in water is more than 30 ns, absurdly 1 order of magnitude larger than that predicted on pure theoretical basis from absorption/emission spectra. These findings imply that the low quantum yield in water cannot be related to an additional nonradiative decay channel from the lowest vibrational level of the excited state (quenching mechanism). This means that, after the fast vertical transition due to excitation, the coumarin can evolve along two different energy landscapes: one is the usual internal conversion down to the lowest vibrational level of the excited state, the other engages a fast (ps) transition to an excited state of different nature (possibly after some internal conversion) that provides a very effective de-excitation pathway down to ground state (Figure 6). On account of recent results described for similar coumarin structures,[65] we are tempted to identify this second excited state to a twisted intramolecular charge transfer (TICT) configuration. DFT calculations show the electronic transition of **1a** to be associated with a significant rearrangement of electronic charge,

(65) Satpati, A. K.; Kumbhakar, M.; Nath, S.; Pal, H. *Photochem. Photobiol.* **2009**, *85*, 119–129.

in a typical ICT fashion. Usually ICT may evolve to TICT if the interactions with the solvent molecules are favorable to the latter configuration. Indeed, there is evidence for similar coumarin systems in which a TICT state can be stabilized by the establishment of strong H-bonding interactions with water molecules. This would explain the high sensitivity of fluorescence emission of our compounds from the H-bonding capability of the surrounding medium.

The solvatochromic behavior of **1e** is richer. First of all, the quantum yield of emission shows good correlation with solvent polarity (Figure 2a), and therefore, the brightness enhancement relative to water is solvent dependent (Figure 2b). This correlation is lost for pure water. More, **1e** has constantly poor emission in all of the polarity range where its non-cyano counterpart **1a** shows a sudden increase of brightness (Figure 2c). Below a certain polarity value ($\Delta f \approx 0.31$), however, the brightness of **1e** is linearly related to Δf, following a "Lippert−Mataga" behavior. These findings suggest that **1e** has a solvent-dependent emission related to a differential stabilization of ground and excited states below a certain polarity level, and it is dark otherwise. Accordingly, the lifetime of **1e** in water/*i*-PrOH mixtures is strictly linear with Δf except for pure water (τ_{550}, Figure 2f). The dual fluorescence of **1e** upon <400 nm excitation is conserved in all solvents. Nonetheless, the relative ratio between the two emission bands is polarity-dependent (Figure 2d). This behavior is particularly evident for water/organic solvent mixtures and supports the use of **1e** as a ratiometric probe of polarity. Note that in water only the high-energy emission band is present ($\tau_{sh} \approx 470$ nm, Figure 2d). The dual fluorescence is reflected also in a biexponential (i.e., bicomponent) lifetime decay. The deconvolution of the decay curves yielded the lifetime associated with the high-energy emission band (τ_{470}). Importantly, τ_{470} resulted independent of medium polarity including also water. Thus, the high-energy band of **1e** looks very similar in wavelength and lifetime behavior to the emission of its non-cyano parent **1a**. These data support a photophysical model encompassing two communicating excited states similar to that described for non-cyano coumarins (Figure 6). The major difference, however, resides in the existence of radiative channels from both excited states. Additionally, the efficiency of the transition from the low-energy excited state is polarity-dependent. Although we may be tempted to attribute the two excited states to ICT and TICT in analogy with non-cyanocoumarins, the complexity of the photophysical pattern requires further investigation to provide a reliable hypothesis, and this topic will be the subject of a forthcoming paper.

Finally, we investigated the photophysical behavior and the localization of our compounds in cultured cells. Our goals were to verify that: (1) the compounds can be efficiently imaged in a typical confocal microscope setup; (2) the photophysical properties assessed *in vitro* are not distorted by the biological environment; (3) the compounds do not prevent cell viability; (4) in cell environments enriched in water (e.g., cytoplasm) the fluorescence is low. We found that all these requirements are met. Indeed, after administration to cultured cells, the confocal analysis showed that the coumarins stained lipophilic cellular subdomains (Figure 3a,b, and 4). Conversely, our compounds were almost nonfluorescent in cytoplasm, nucleoplasm, and external buffer media. The photophysical properties in living cells are completely superimposable on those *in vitro* in terms of emission spectra and lifetime decays (Figure 3c). In particular, **1e** shows a polarity-dependent lifetime that allows identifying clearly the relative lipophilicity of different subcellular domains (Figure 3e,f). Cells were found to be viable for at least 2−3 h, indicating the low toxicity of the coumarins. It is worth noting, however, that future bioapplications will involve much lower concentrations and the conjugation will be with specific biomolecules so as to further reduce any toxic effect.

Even though future application of the dyes will involve conjugation to biomolecules that will act as carriers for our coumarins to specific domains, the peculiar staining showing in the cells (Figure 3a,b) prompted us to achieve a better insight in the distribution of our fluorescent probes. Colocalization with standard organelle markers evidenced similar, albeit not identical, distribution in the cells. In particular, both **1a** and **1e** were extensively sequestered in endoplasmic reticulum (Figure 4c,d); additionally, **1e** also stained more lipophilic domains such as membranes and lysosomes (Figure 4b,f). This different subcellular distribution can be evidenced by plotting the ratio of the signal of the two dyes, concomitantly administered to the cells, and it is in keeping with the different log *P* of the two probes.

4. Conclusions

In this work, we targeted the rational design and engineering of a modular toolbox of polarity-sensitive probes to be used as indicators of biochemical processes involving the change of environmental polarity. One good example is the binding between two biomolecules (e.g., two proteins) and the radical variation of polarity at the interface of contact. In such cases, polarity probes are thought to circumvent some of the critical issues related to conventional FRET biosensors.

Our goal was accomplished by following a stepwise procedure. First, we selected a photophysically promising chemical structure, namely donor−(coumarin core)−acceptor where alkylethers or naphthyl played the role of electron donors and benzothiazene ring and cyano the role of electron acceptors. *In silico* screening allowed identifying good substituent configurations for imaging in the visible region of spectrum. The selected structures were synthesized in high yields by means of a flexible and straightforward procedure that is insensitive to the nature of the reactants. Hence, future functional derivatives will require only an appropriate choice of the reactants. Most of the prepared compounds showed good to excellent fluorescent properties for imaging applications in terms of Stokes' shift and brightness.

In terms of solvatochromism, we obtained two classes of compounds. Coumarins devoid of a conjugated cyano group were found to behave as polarity switches. They are almost nonfluorescent in water or bioenvironments enriched in water, but they sharply become very emissive once the polarity of the environment falls below a certain level. On account of our experimental data, we believe that this effect is associated with a strong H-bonding stabilization by water molecules of a TICT excited state, accessible from the original excited state, and possessing a very efficient nonradiative decay channel. Preliminary results yet to be published show that this effect is maintained also when the coumarin is linked to a protein structure.

A cyanocoumarin was found to exhibit a rich photophysical behavior, very dependent on environment polarity. In particular, this compound is a promising concentration-independent indicator of intracellular polarity on account of its spectral ratiometric behavior when excited around 400 nm and its polarity-modulated mono-exponential lifetime when excited above 450 nm.

Finally, tests of our compounds in cultured cells revealed that they are very suitable for *in vivo* high-resolution microscope imaging in both spectral and lifetime modes. We believe that these compounds, after appropriate functionalization and conjugation to target biomolecules, will represent remarkable tools to investigate subtle biochemical processes in the cell environment. Furthermore, the photophysical comprehension of the environmental sensitivity displayed by our coumarins will allow for the engineering of further compounds tailored to specific applications. Studies in both directions are currently under way.

Acknowledgment. We gratefully acknowledge Prof. Fabio Beltram for precious scientific suggestions during the research work and in preparing this manuscript and Dr. Paolo Facci for stimulating discussions. This work was supported by INFM-CNR under the framework of Seed Project "Solvatochromic fluorescent dyes for bulk and single-molecule detection of intracellular native proteins". The partial support of the Italian Ministry for University and Research (MiUR) under the framework of the FIRB project RBLA03ER38 is also acknowledged.

Supporting Information Available: Detailed synthetic procedures; ^{1}H and ^{13}C NMR spectra for all compounds; spectroscopic data and high-resolution mass spectra for all compounds; complete ref 53. This material is available free of charge via the Internet at http://pubs.acs.org.

JA9050444